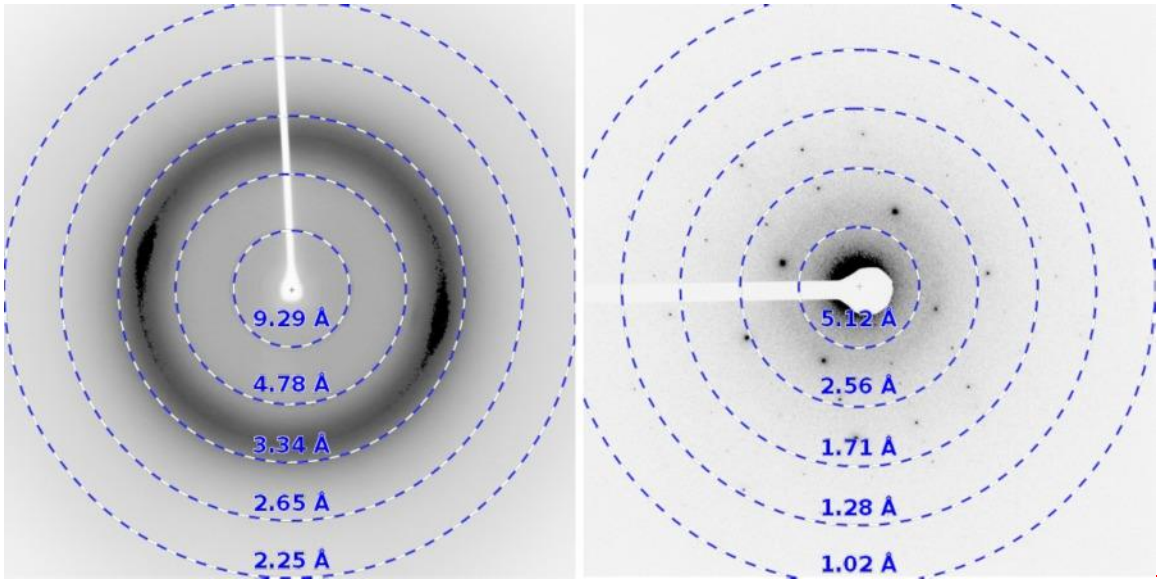

Supplementary Figure 1

X-ray and corresponding MicroED diffraction pattern from protein tau.

(Left) When extracted from hanging drops, a cluster of microneedle crystals of the amyloid-forming protein tau diffracts as powder to no better than 4.2 Å using a rotating anode X-ray source. Physically breaking these needle clusters and selecting individual sub-micron thick crystal fragments yields diffraction to atomic resolution by MicroED (right) and a structure solvable by direct methods. The X-ray diffraction pattern was collected over a 6° oscillation range; the MicroED pattern spans a 0.6° wedge. See main text for data collection details.

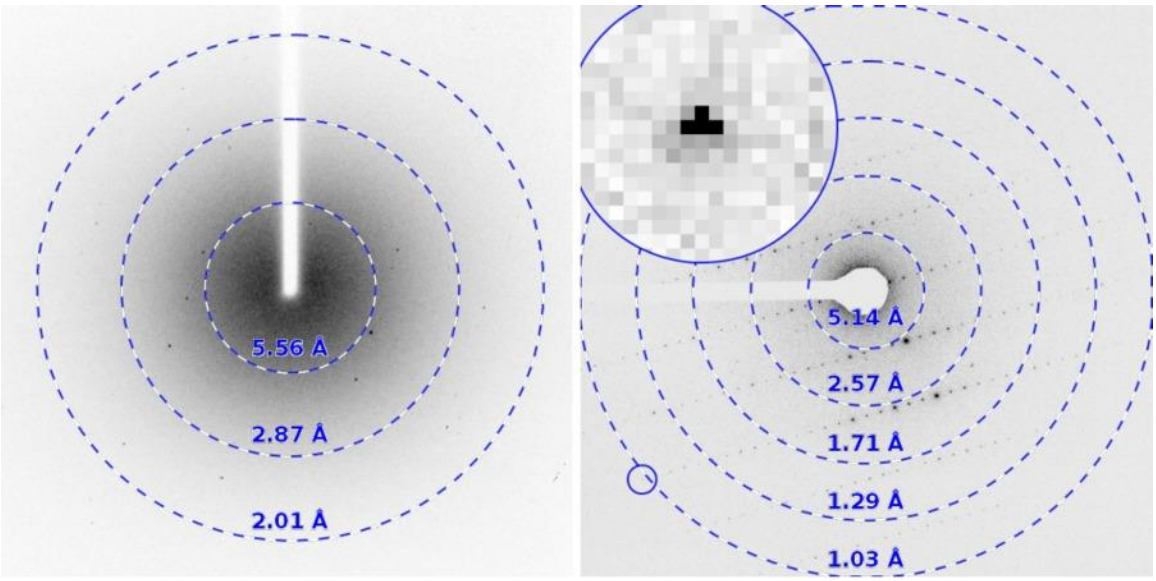

Supplementary Figure 2

X-ray and corresponding MicroED diffraction pattern from Zn^{2+}-NNQQNY.

The structure has previously been solved by X-ray diffraction, albeit at lower resolution [Nelson *et al.* (2005) Nature **435**, 773–778]. It was readily redetermined by direct methods from the MicroED data [Sawaya *et al.* (2016) Proc Natl Acad Sci **113**, 11232–11236]. For the MicroED pattern the inset shows a close-up of the spot indicated by the blue circle.

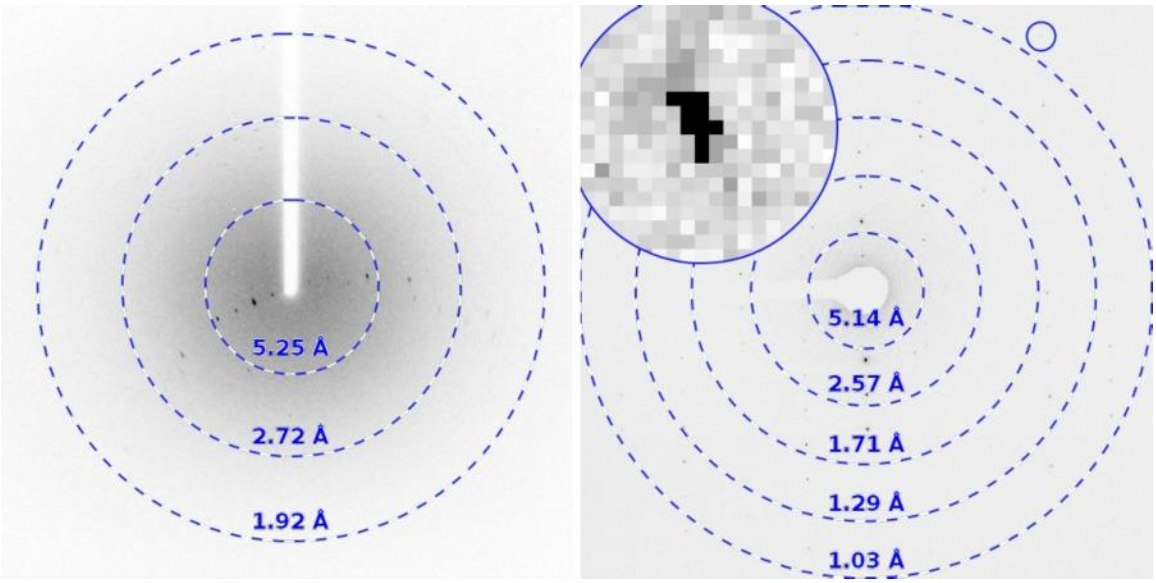

Supplementary Figure 3

X-ray and corresponding MicroED diffraction pattern from Cd^{2+}-NNQQNY.

This structure was not previously solved by X-ray diffraction, but was readily determined by direct methods from the MicroED data [Sawaya *et al.* (2016) Proc Natl Acad Sci **113**, 11232–11236]. For the MicroED pattern the inset shows a close-up of the spot indicated by the blue circle.

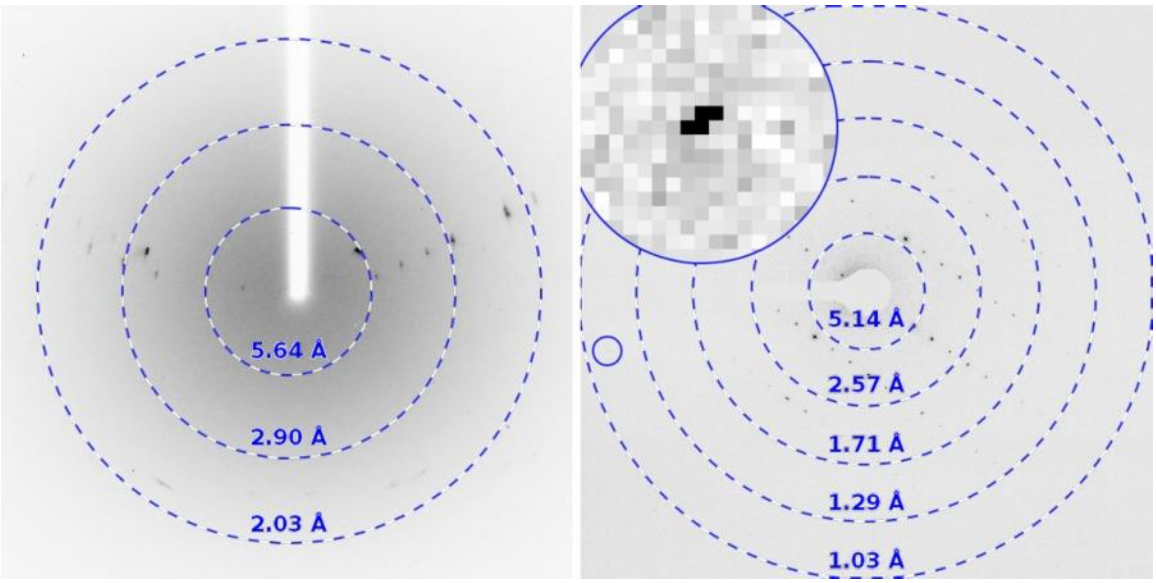

Supplementary Figure 4

X-ray and corresponding MicroED diffraction pattern from GNNQQNY.

The structure has previously been solved by X-ray diffraction, albeit at lower resolution [Nelson *et al.* (2005) Nature **435**, 773–778]. It was readily redetermined by direct methods from the MicroED data [Sawaya *et al.* (2016) Proc Natl Acad Sci **113**, 11232–11236]. For the MicroED pattern the inset shows a close-up of the spot indicated by the blue circle.

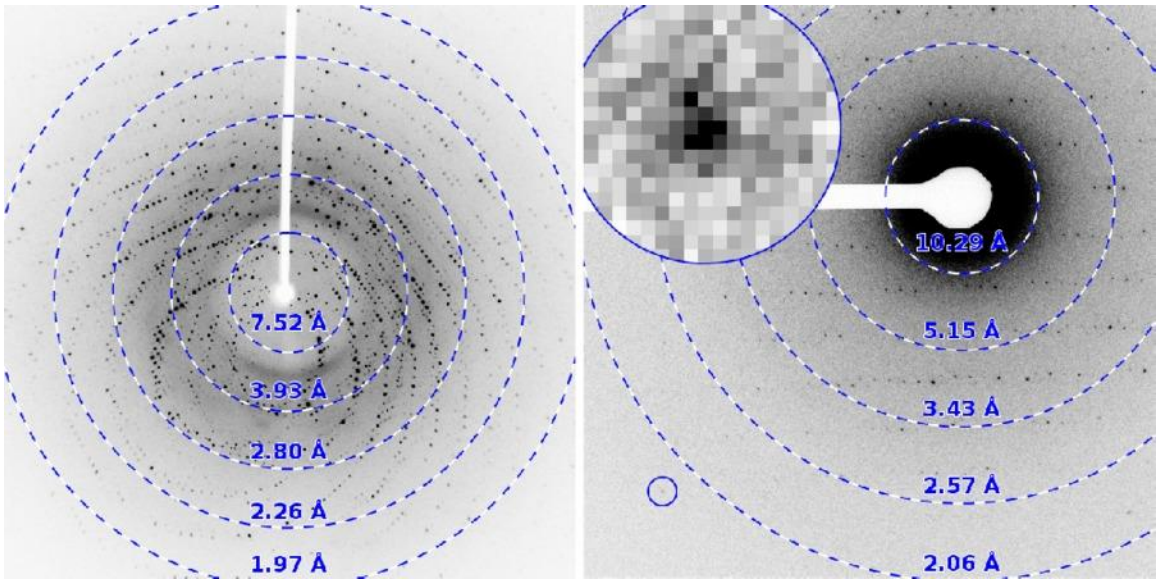

Supplementary Figure 5

X-ray and corresponding MicroED diffraction pattern from lysozyme.

The X-ray diffraction pattern displays multiple lattices. No optimization of crystal growth was done; instead crystals were sonicated and probed by MicroED. The obtained resolution was as good as what was obtained from the parent crystal. For the MicroED pattern the inset shows a close-up of the spot indicated by the blue circle.

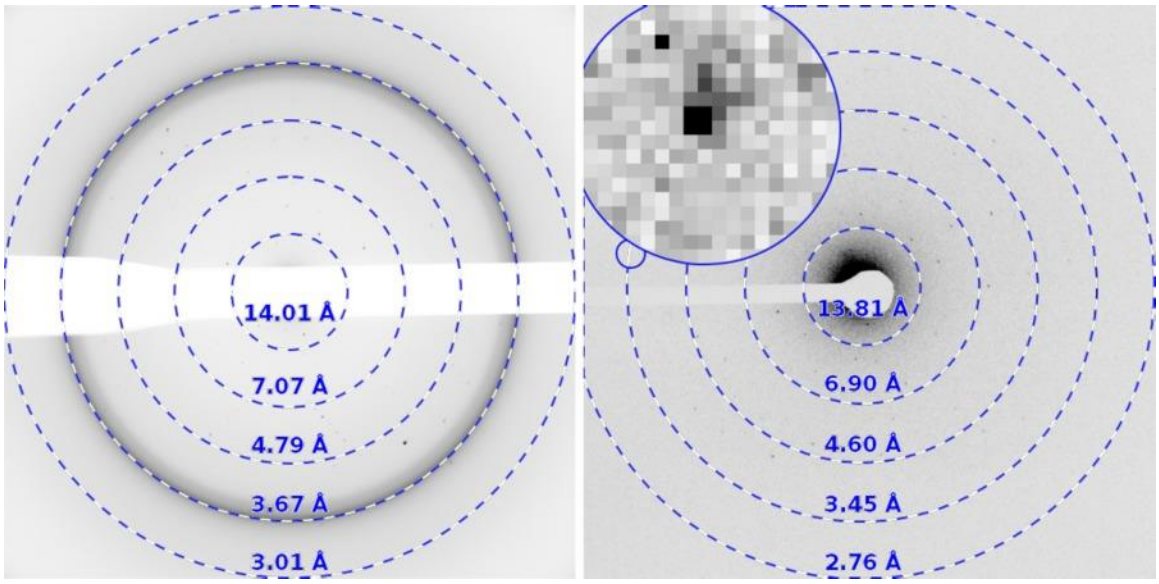

Supplementary Figure 6

X-ray and corresponding MicroED diffraction pattern from TGF-βm–TβRII.

The X-ray diffraction pattern was collected at an X-ray free-electron laser, but the crystals diffracted better under MicroED. No optimization of crystal growth was done; instead crystals were vortexed with glass beads and then probed by MicroED. For the MicroED pattern the inset shows a close-up of the spot indicated by the blue circle.

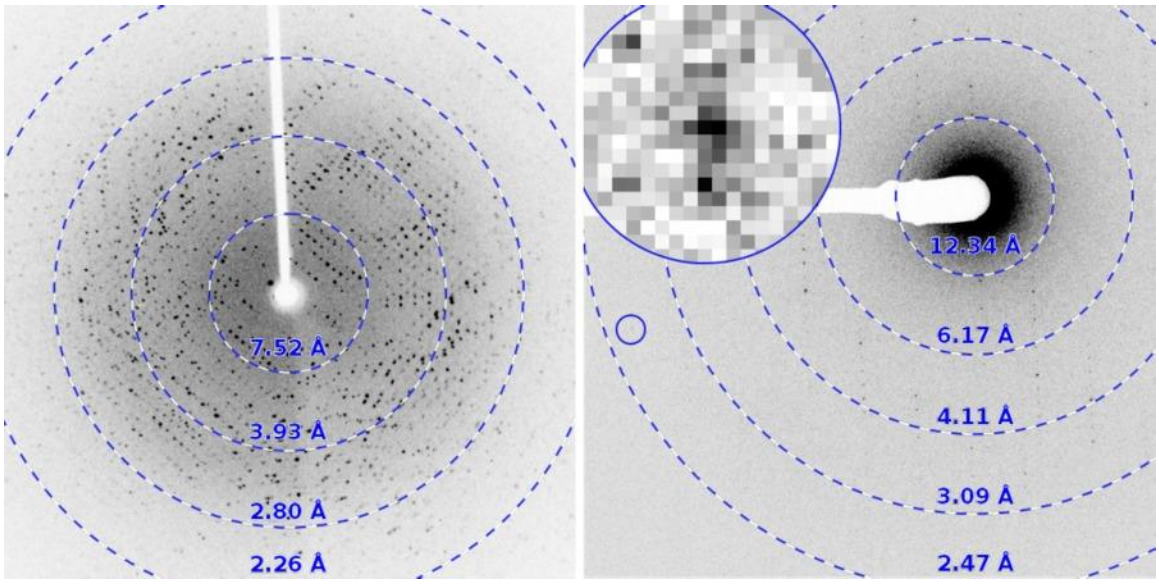

Supplementary Figure 7

X-ray and corresponding MicroED diffraction pattern from xylanase.

The X-ray diffraction pattern displays several multiple lattices. No optimization of crystal growth was done; instead crystals were sonicated and probed by MicroED. The obtained resolution was as good as what was obtained from the parent crystal. For the MicroED pattern the inset shows a close-up of the spot indicated by the blue circle.

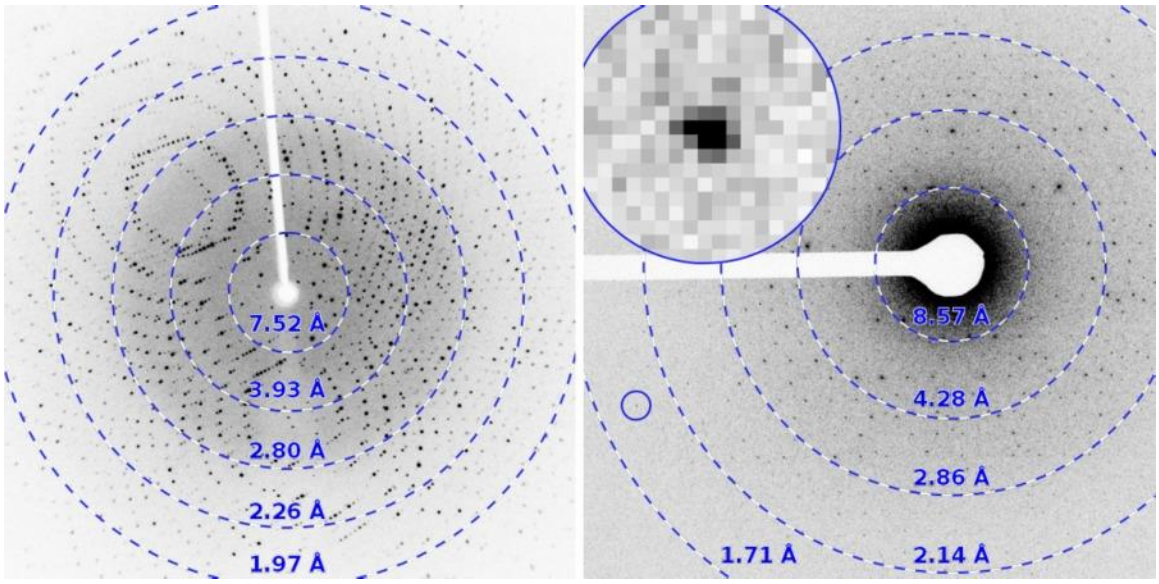

Supplementary Figure 8

X-ray and corresponding MicroED diffraction pattern from proteinase K.

The X-ray diffraction pattern displays multiple lattices. No optimization of crystal growth was done; instead crystals were sonicated and probed by MicroED. The obtained resolution was better than what was obtained from the parent crystal. For the MicroED pattern the inset shows a close-up of the spot indicated by the blue circle.

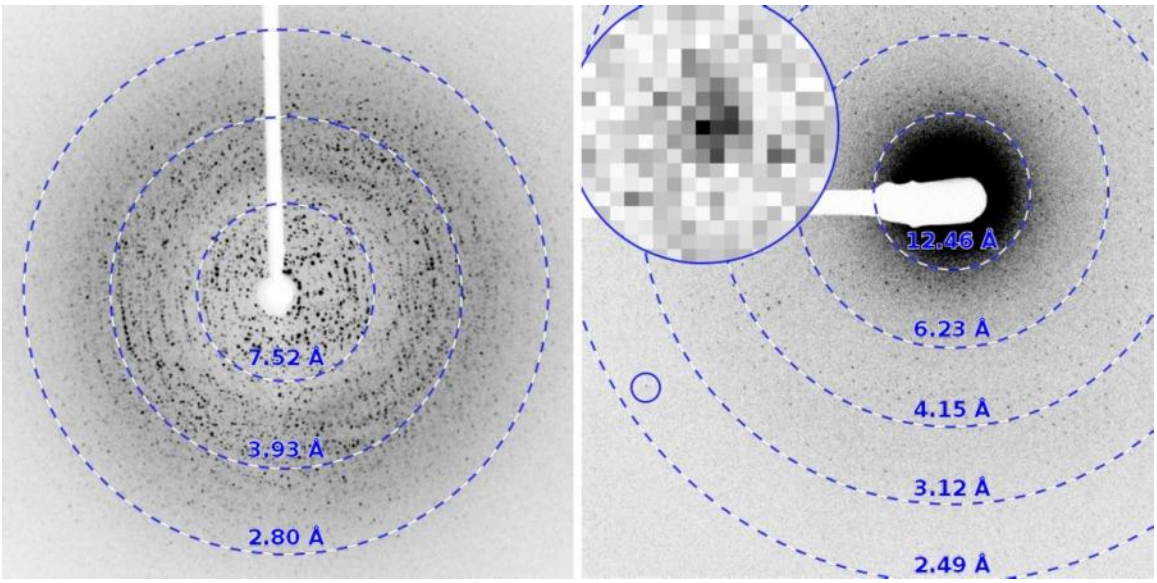

Supplementary Figure 9

X-ray and corresponding diffraction pattern from thermolysin.

The X-ray diffraction pattern is powder-like. No optimization of crystal growth was done; instead crystals were sonicated and probed by MicroED. The obtained resolution was better than what was obtained from the parent crystal. For the MicroED pattern the inset shows a close-up of the spot indicated by the blue circle.

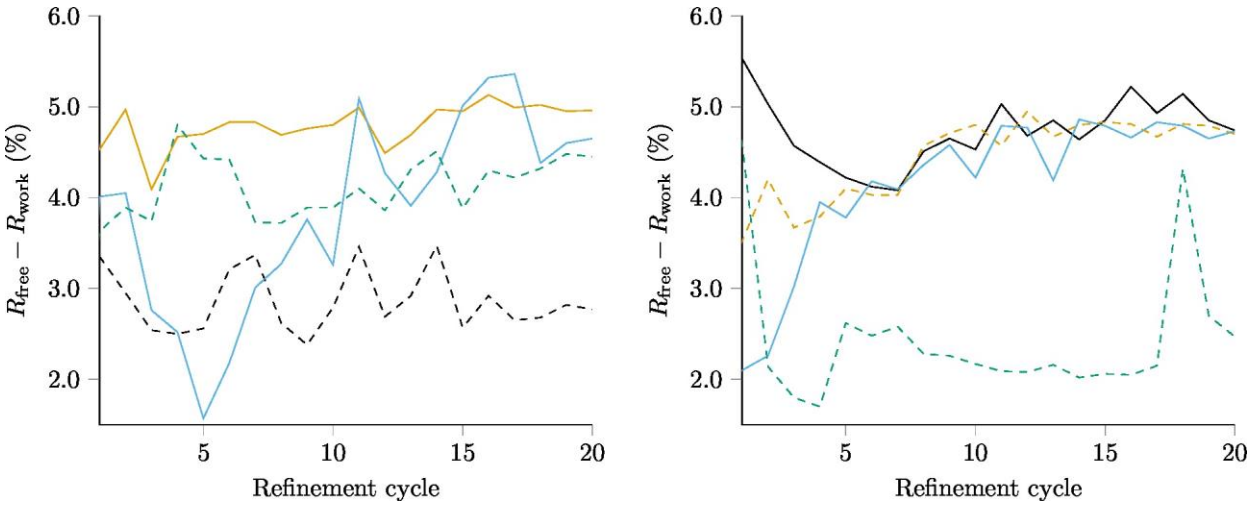

Supplementary Figure 10

R_{free} – R_{work} as a function of refinement cycle.

The *R*-factor gap is always less than 6% and the variation is generally within ±1% after the first few cycles. The variation is greater for TGF-βm–TβRII, thaumatin, and thermolysin, which are the lowest-resolution structures in this study. (Left) tau peptide (dashed black curve), lysozyme (solid orange curve), TGF-βm–TβRII (solid blue curve), and xylanase (dashed green curve). (Right) thaumatin (solid black curve), trypsin (dashed orange curve), proteinase K (solid blue curve), and thermolysin (dashed green curve). All refinements were performed using *phenix.refine* [Afonine *et al.* (2012) Acta Crystallogr D Biol Crystallogr **68**, 352–367].

Sample (PDB id; EMDB id)	Tau peptide (5k7n; EMD-8216)	Lysozyme (5k7o; EMD-8217)	TGF-βm:TβRII (5ty4; EMD-8472)	Xylanase (5k7p; EMD-8218)	Thaumatin (5k7q; EMD-8219)	Trypsin (5k7r; EMD-8220)	Proteinase K (5k7s; EMD-8221)	Thermolysin (5k7t; EMD-8222)
	Data collection							
Resolution (Å)	14.70–1.10	30.58–1.50	26.64–2.90	25.55–1.90	27.73–2.11	27.63–1.50	20.75–1.30	30.14–1.60
# crystals	2	7	3	4	3	10	6	4
<$T_{exposure}$> (s)	159.9	127.7	140.8	172.7	179.7	155.8	122.2	187.6
Molecular weight (kDa)	0.7	14.4	19.1	21.0	22.2	23.4	28.9	34.6
	Data processing							
Resolution[1] (Å)	14.70–1.10 (1.23–1.10)	30.58–1.80 (1.84–1.80)	26.64–2.90 (3.07–2.90)	25.55–2.30 (2.38–2.30)	27.73–2.51 (2.61–2.51)	27.63–1.70 (1.73–1.70)	20.75–1.60 (1.63–1.60)	30.14–2.50 (2.61–2.50)
Space group	*C*121	$P4_32_12$	$P2_12_12_1$	$P2_12_12_1$	$P4_12_12$	$P2_12_12_1$	$P4_32_12$	$P6_122$
Unit cell								
a, b, c (Å)	29.42, 4.99, 37.17	76.23, 76.23, 37.14	41.53, 71.33, 79.51	48.16, 59.75, 69.81	58.12, 58.12, 150.31	53.18, 56.43, 64.67	67.06, 67.06, 100.71	92.07, 92.07, 128.50
α, β, γ (°)	90, 111.55, 90	90, 90, 90	90, 90, 90	90, 90, 90	90, 90, 90	90, 90, 90	90, 90, 90	90, 90, 120
# total reflections[1]	6,185 (463)	88,734 (2,330)	14,911 (2,371)	32,523 (1,675)	39,272 (3.353)	137,532 (1,999)	246,199 (7,172)	137,511 (13,673)
# unique reflections[1]	3,319 (255)	10,372 (567)	3,884 (614)	7,774 (578)	8,868 (920)	19,843 (709)	29,968 (1,308)	11,203 (1,138)
$CC_{1/2}$[1]	0.987 (0.639)	0.901 (-0.013)	0.951 (0.255)	0.918 (0.052)	0.848 (0.071)	0.722 (0.071)	0.912 (0.051)	0.847 (0.201)
$\langle I/\sigma_I \rangle$[1]	2.4 (1.1)	3.7 (0.8)	3.3 (0.8)	3.5 (1.0)	3.5 (1.8)	2.6 (0.3)	3.4 (0.9)	5.6 (3.8)
Completeness[1]	83.0 (79.4)	97.6 (93.2)	71.9 (71.3)	85.4 (66.1)	94.2 (90.0)	90.1 (61.2)	96.8 (86.8)	97.1 (90.3)
Multiplicity[1]	1.9 (1.8)	8.6 (4.1)	3.8 (3.9)	4.2 (2.9)	4.4 (3.6)	6.9 (2.8)	8.2 (5.5)	12.3 (12.0)
	Refinement							
Resolution[1] (Å)	14.70–1.10 (1.12–1.10)	30.59–1.80 (2.06–1.80)	26.64–2.90 (3.65–2.90)	25.55–2.30 (2.63–2.30)	27.73–2.50 (2.86–2.50)	25.86–1.70 (1.79–1.70)	20.75–1.60 (1.64–1.60)	30.14–2.50 (2.75–2.50)
R_{work}[1] (%)	20.97 (21.04)	23.95 (32.33)	29.19 (36.11)	22.95 (35.40)	25.13 (34.08)	24.79 (38.72)	22.35 (36.33)	28.99 (34.78)
R_{free}[1,2] (%)	22.28 (22.43)	28.42 (37.94)	32.80 (36.87)	26.70 (38.95)	29.45 (38.98)	28.11 (42.37)	25.46 (42.25)	30.96 (36.64)
RSCC	0.84	0.89	0.72	0.85	0.86	0.89	0.91	0.86
# residues	6	129	166	190	207	223	279	316
# protein atoms	53	1,001	1,327	1,481	1,551	1,629	2,029	2,432
# water molecules	2	87	0	23	18	195	221	21
# ligand atoms	0	3	0	2	0	2	2	13
<ADP> (Å^2)								
Protein	12.4	13.4	47.8	25.5	20.3	13.9	8.1	4.9
Water	17.3	14.3		19.4	13.3	14.9	13.4	4.2
Ligand		16.7		66.5		19.6	18.9	7.5
R.m.s.d. bonds (Å)	0.012	0.004	0.012	0.002	0.002	0.005	0.004	0.003
R.ms.d. angles (°)	0.770	0.609	1.573	0.496	0.462	0.739	0.663	0.509
Ramachandran (outliers, favored) (%)	0.0, 100	0.0, 97.6	2.5, 89.9	0.0, 96.3	0.0, 95.1	0.0, 96.4	0.4, 96.8	0.0, 94.9

Supplementary Table 1

Data processing and model refinement statistics for the reported crystal structures.

Data sets were collected and processed as described in the online methods section. The dose rate did not exceed 0.01 $e^-/Å^2/s$ and the mean per-crystal exposure time is given as $\langle T_{exposure} \rangle$ for each sample. Except for tau peptide and TGF-βm:TβRII, reflections were initially integrated to the corners of the detector; the final resolution cutoff was determined based on $CC_{1/2}$ and the stability of the refinement procedure.

[1] Numbers in parentheses reflect the highest resolution shell for either data collection or refinement.

[2] In all cases the test set comprises approximately 5% of the unique reflections, where possible chosen to match that of the deposited data for the MR search model.